Micellization of Poly(ethylene oxide)-Poly(propylene oxide) Block Copolymers in Aqueous Solution: Effect of Polymer Polydispersity

Per Linse

Physical Chemistry 1, Chemical Center, University of Lund, P.O. Box 124, S-221 00 Lund, Sweden

Received April 14, 1994; Revised Manuscript Received August 12, 1994[⊗]

ABSTRACT: The effect of polymer polydispersity on micellization in an aqueous solution of triblock copolymers containing ethylene oxide (EO) and propylene oxide (PO) was modeled. A mean-field lattice theory for multicomponent mixtures of copolymers with internal degrees of freedom was applied. The polydisperse polymer was represented as consisting of several components, and a Schulz-Zimm distribution was assumed. The critical micellar concentration (cmc) and the aggregation number number were examined for a number of PEO-PPO-PEO polymers at different temperatures and with different polydispersity ratios. Segment density profiles indicated the polymer micelles to consist of a hydrophobic core composed mainly of PO and an outer layer composed of a mixture of EO and water. The polydispersity led to a reduction in the cmc by several orders of magnitude, which brought experimental and calculated data close to each other. The precise value of the cmc was found to depend strongly on the criterion of the cmc. The polydispersity also led to an increase in micellar size, a greater separation of the EO and PO segments, and a marked decrease in micellar size with increasing total polymer concentration. The fractions of the different polymer components of the micelles depended strongly on the polymer concentration. Close to the cmc, the micelles were predominantly formed by the longest components, which had the lowest cmc. At high polymer concentrations, the intermicellar solution became strongly depleted of the long polymer components. The strong temperature dependence of the cmc and of the aggregation number was not changed essentially by polydispersity.

I. Introduction

In recent years the physico-chemical properties of aqueous solutions of triblock copolymers of the PEO-PPO-PEO type [PEO and PPO are poly(ethylene oxide) and poly(propylene oxide), respectively] have been the subject of a number of investigations, experimental[1-18] as well as theoretical.[19-25] These polymers are often referred to by their trademarks Pluronic, Proxanol, and Synperonic, and the term Pluronic will be used here. The Pluronic polymers have an amphiphilic character due to the PPO block being more hydrophobic and the PEO block being more hydrophilic. They are able to self-aggregate in aqueous solution and form an isotropic micellar solution, but also liquid crystalline and cubic phases have recently been reported.[9,12,17,18] The properties of Pluronic polymers in aqueous solution thus resemble those of nonionic surfactants of the alkyl poly(ethylene oxide) type. They differ from the latter, however, by their solubility decreasing strongly as the temperature increases. As a result, a given phase transition can be induced by either an increasing/decreasing temperature or an increasing/decreasing polymer concentration.

In addition, the transition from the monomeric state to the micellar state in an aqueous solution of Pluronic polymers is more gradual than in nonionic surfactant solutions. The critical micellar concentrations (cmc's) and the aggregation numbers reported for the Pluronic polymers differ substantially from case to case, however, due to polymer impurities[3,8] and to substantial polydispersity,[5,26] both being a consequence of the manufacturing process. The aim of the present investigation is to examine theoretically the influence of polydispersity on the micellization process. The study represents a continuation of earlier work on how micellization is affected by the polymer composition and structure of block copolymers containing EO and PO,[21] as well as by the presence of both PEO and PPO homopolymer and of PPO-PEO diblock copolymer impurities.[25] Closely related is also earlier work, involving the same theoretical approach, on the phase behavior of aqueous solutions of different Pluronic polymers.[24] Hurter et al. have employed this approach too in studying the solubilization of small hydrophobic molecules in Pluronic micelles.[23]

It was found in two of the earlier studies[21,24] that the predicted critical micellar temperature curves were located ≈20-30 K above the experimental ones and, moreover, that micellization could not be predicted for a short polymer of the Pluronic family. It was suggested that the presence of polydispersity, in particular, and also of impurities in the experimental samples could be the cause of those discrepancies. In ref 25 it was found that the impurities indeed reduced the cmc, or alternatively, the critical micellar temperature (cmt), but that the effect was smaller than the discrepancies just referred to. As will be shown here decisively, polydispersity has a stronger influence on the cmc than impurities do. A polydispersity ratio of 1.2 can cause a reduction in the cmc by several orders of magnitude.

In addition to considering Pluronic polymer systems as such, the present study examines the general phenomenon of the preferential self-aggregation of different polymer fractions in polydisperse polymer samples. A thermodynamic theory presented by Gao and Eisenberg[27] is applicable here. Selective behavior of a sort similar to that described has also been predicted for adsorption on solid surfaces.[28,29]

The theoretical approach used here is based on a lattice theory for heterogeneous systems, developed initially by Scheutjens and Fleer[30] and later extended to apply to micelle formation[31] and to polymers possessing internal degrees of freedom.[32] This approach provides a formalism allowing temperature and concentration dependent interaction parameters to be obtained using a conformational model originally developed by Karlström.[33] Such a polymer

[⊗] Abstract published in *Advance ACS Abstracts*, September 15, 1994.

0024-9297/94/2227-6404$04.50/0

model has been used successfully for describing the inverse temperature behavior of aqueous solutions of PEO and related polymers (for which a worsening of the solvency condition occurs when the temperature increases, this often leading to phase separation). The conformational model accounts for the fact that the various conformations of ethylene oxide groups differ in their dipole moments and that polar conformations are infrequent among them. The conformations that occur can be divided into two classes or states, one more polar and of lower energy level, the other less polar (referred to as nonpolar) and of higher statistical weight. At low temperatures the former class dominates, the effective polymer–solvent interaction being favorable, whereas at higher temperatures the latter class becomes more important, making the polymer–solvent interaction more unfavorable. An increase in the polymer concentration also makes the effective polymer–solvent interaction more unfavorable.

The paper is organized as follows. The theory basic to the heterogeneous lattice model for polymers with internal degrees of freedom is outlined briefly in section II, in which an account is also provided of the thermodynamic model which applies to micellization. Section III deals with the polymer model and with the interaction parameters used in the investigation. In particular, extension to the polydisperse case is discussed, and two cases of polydispersity are considered, one a case of mass polydispersity with a constant EO/PO composition and the other a case of independent polydispersity of the different blocks. In both cases the polydisperse polymer is considered as consisting of components of differing length (and composition). In section IV, calculated results are presented. Considered there initially is the convergency of the polydispersity expansion. Results concerning the micellar structure, the temperature dependence, and the polydispersity dependence of the micellization of Pluronic P105 occurring in aqueous solution are then presented. Thereafter, the effects of the mass and composition polydispersity of Pluronic P105 are examined. The final parts of section IV deal with the polydispersity of a reversed Pluronic polymer, of Pluronic L64, and of F127. The paper ends with section V, which presents a summary of the major conclusions.

II. Theory

The conditions for the existence of (locally) stable micellar aggregates, as well as the size and structure of the micelles, were examined using a lattice theory for multicomponent mixtures of copolymers with internal degrees of freedom.[32] Since the theory employed here and the set of interaction parameters used are the same as in the previous investigations of micellization of Pluronic polymers,[21] these matters will be dealt with only briefly here, except for the discussion in some detail of how the theory has been adapted for calculations concerning multicomponent micelles. For a more detailed description of the lattice theory used, see, e.g., refs 30–32.

The space is divided into concentric shells, and each shell is further divided into lattice cells, one polymer segment or a solvent molecule contained in each. The conformations of a polymer chain are described as random walks on the spherical lattice; see Figure 1. Interactions are regarded as extending only to segments or solvent molecules in adjacent lattice cells. The random-mixing (mean-field) approximation is applied within each layer separately, making it possible to obtain radial concentration profiles.

The computations involve the self-consistent determination of *state* distributions (i.e., the distributions of the polar and nonpolar states of the EO and PO species in each layer) and *segment* distributions (i.e., the radial distribution of each polymer segment and of the water molecules). The state distribution, derived from the partition function, is given by the following implicit set of nonlinear equations[32]

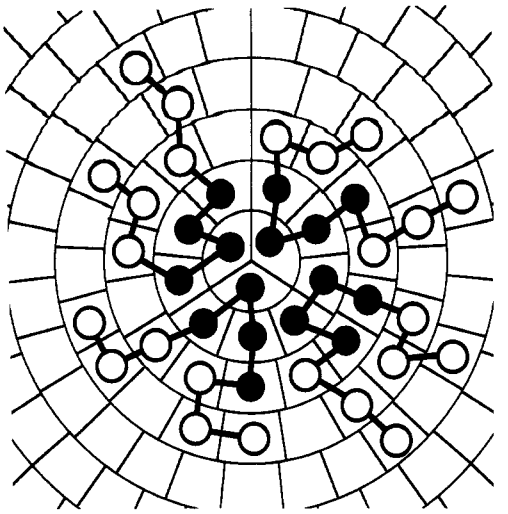

Figure 1. Two-dimensional illustration of an infinite sherical lattice and a micelle composed of four triblock copolymers, $B_3A_4B_3$. The hydrophobic segments A (filled circles) form the central part of the micelle, whereas the more hydrophilic segments B (open circles) form the outer layer of the micelle. Note the small number of unfavorable contacts between the hydrophobic segments and the solvent (unfilled lattice cells).

$$P_{ABi} = \frac{X_{AB}}{\sum_{B} X_{AB}}$$

$$X_{AB} \equiv g_{AB} \exp[-\beta U_{AB} - \sum_{A'} \sum_{B'} \chi_{BB'} \langle P_{A'B'i} \phi_{A'i} \rangle] \quad (1)$$

valid for all species (EO, PO, and water, collectively labeled A), states (polar and nonpolar conformation in the case of EO or PO, collectively labeled B), and layers (i). In eq 1, P_{ABi} denotes the fraction of species A in layer i which is in state B, U_{AB} is the internal energy of state B of species A (arising from the difference in internal energy between the polar and nonpolar conformations), g_{AB} is the degeneration factor of state B of species A (arising from the difference in the numbers of polar and nonpolar conformations), $\chi_{BB'}$, is the Flory–Huggins interaction parameter representing the interaction between species A in state B and species A′ in state B′, and ϕ_{Ai} is the volume fraction of species A in layer i. Moreover, $\beta = (kT)^{-1}$, where k is the Boltzmann constant and T the absolute temperature. The angular brackets indicate an averaging over three adjacent layers. Thus, a given state is favored by high degeneration, low internal energy, and favorable interaction (small χ) with its neighboring segments.

The species volume fraction ϕ_{Ai} needed in eq 1 is directly related to n_{xsi}, the number of sites in layer i occupied by segments of rank s (the sth segment in the chain) belonging to component x, in accordance with

$$\phi_{Ai} = \frac{1}{L_i} \sum_{x} \sum_{s=1}^{r_x} \delta_{A,t(x,s)} n_{xsi} \quad (2)$$

where L_i is the number of sites in layer i and r_x is the number of segments in component x. The Kronecker delta

selects only segments of rank s of component x if they are of type A. The components considered in the present investigations are water and the polymer components which represent the polydisperse Pluronic polymer.

The expression for the segment distribution is more complex, since the correct weight of all conformations, as well as the connectivity of the chains, has to be taken into account. Again, starting with the partition function, n_{xsi} is obtained using a matrix method and is given by[32]

$$n_{xsi} = C_x \{\Delta_i^T \cdot [\prod_{s'=r_x}^{s+1} (\mathbf{W}^{t(x,s')})^T] \cdot \mathbf{s}\} \{\Delta_i^T \cdot [\prod_{s'=2}^{s} \mathbf{W}^{t(x,s')}] \cdot \mathbf{p}(x,1)\} \quad (3)$$

where C_x is a normalization factor related to the bulk volume fraction of component x, $\mathbf{W}^{t(x,s)}$ is a tridiagonal matrix comprising elements which contain factors describing the lattice topology as well as weighting factors for segment of rank s belonging to component x, and $\mathbf{p}(x,1)$ is a vector describing the distribution of the first segment of component x among the layers, Δ and $\mathbf{s}$ being elementary column vectors. In the present study, a hexagonal lattice involving 12 nearest neighbors has been selected. The weighting factor G_{Ai} for species A in layer i entering $\mathbf{W}$ is given by

$$G_{Ai} = \exp(-\beta u_{Ai}) \quad (4)$$

where the species potential u_{Ai} can be divided into two parts according to

$$u_{Ai} = u'_i + u_{Ai}^{int} \quad (5)$$

If the species potentials are defined with respect to the bulk solution, i.e., if $u_A^b = 0$, then the two terms are given by

$$\beta u'_i \equiv \alpha_i + \sum_x \frac{\phi_x^b}{r_x} + \frac{1}{2}\sum_{A'}\sum_{A''}\sum_{B'}\sum_{B''} \phi_{A'}^b P_{A'B'}^b \chi_{B'B''} P_{A''B''}^b \phi_{A''}^b$$

$$\beta u_{Ai}^{int} \equiv \sum_B \left[P_{ABi}\left(\beta U_{AB} + \ln \frac{P_{ABi}}{g_{AB}}\right) - P_{AB}^b \left(\beta U_{AB} + \ln \frac{P_{AB}^b}{g_{AB}}\right)\right] + \sum_{A'}\sum_B\sum_{B'} \chi_{BB'} (P_{ABi}\langle P_{A'B'i}\phi_{A'i}\rangle - P_{AB}^b P_{A'B'}^b \phi_{A'}^b) \quad (6)$$

The species independent term u'_i ensures that the space is completely filled in layer i if a suitable choice is made of α_i, u'_i being related in a continuous model to the lateral pressure. In bulk, u' becomes zero. The species dependent term u_{Ai}^{int} has two contributions: the internal free energy for species A in layer i being diminished by the corresponding quantity in bulk, and the mixing energy for species A in layer i being diminished by the mixing energy for species A in bulk. In both cases, averages are taken over the relevant state distributions. At distances far from the center of the aggregate, P_{ABi} approaches P_{AB}^b, ϕ_{Ai} approaches ϕ_A^b, and hence u_{Ai}^{int} becomes zero. Since u_{Ai} is needed for obtaining ϕ_{Ai} using eqs 2–4, and since u_{Ai} depends in turn on ϕ_{Ai} according to eqs 5 and 6, eqs 2–6 need to be solved self-consistently. In addition, the state distribution, which enters in eq 6 and depends on ϕ_{Ai}, has to fulfill eq 1.

The solution of eqs 1–6 has two branches, one corresponding to homogeneous concentration profiles being formed throughout the lattice and the other to a single micelle, formed at the center of the lattice and in equilibrium with specified bulk concentrations of the components. The free energy of forming the micelle at a fixed position, A^σ, is obtained from the volume fraction distributions of the species and of the states and from the chemical potentials of the components in bulk according to eqs 2–6, 14, and 15 in ref 21. At equilibrium $A^\sigma(>0)$ is balanced by a negative mixing entropy $kT \ln (V_m/V_s)$, where V_m is the volume of the micelle and V_s is the volume of a subsystem containing one micelle and its accompanying solution. The micellar volume is approximated by

$$V_m = \frac{\sum'_x \Gamma_x}{\sum'_x \phi_{x,i=1} - \sum'_x \phi_x^b} \quad (7)$$

where the prime restricts the summation to the polymer components, which constitute the micelle, and Γ_x is the excess number of segments of component x in the subsystem (given by eq 16 in ref 21). The *total* volume fraction of component x in the subsystem (equal to the stoichiometric concentration of x in the micellar solution) is the sum of the excess and bulk volume fractions according to

$$\phi_x^{tot} = \frac{\Gamma_x}{V_s} + \phi_x^b \quad (8)$$

For a selected bulk composition $\{\phi_x^b\}$, the numerical procedure involves the computation of the equilibrium state and segment distributions according to eqs 1–6, whereupon the excess free energy of the subsystem, A^σ, as well as the set of excess numbers of segments of the components $\{\Gamma_x\}$, are calculated. Subsequently, eq 7 provides the micellar volume which together with A^σ and the requirement of equilibrium gives V_s. Finally, the total composition $\{\phi_x^{tot}\}$ is obtained from eq 8. Any change in the bulk composition $\{\phi_x^b\}$ leads to a change in the total composition. The desired $\{\phi_x^{tot}\}$, which for the polydisperse case will be discussed further in the following section, was efficiently obtained by varying $\{\phi_x^b\}$, using a Newton–Raphson scheme.

The aggregation number of a micelle formed by a monodisperse polymer is given in simple terms by $N_{agg} = \Gamma_{polymer}/r_{polymer}$, i.e., the excess of the polymer segments divided by the number of segments of a single chain. In the case of a polydisperse polymer, an effective aggregation number is defined by

$$N_{agg}^{eff} = \frac{\Gamma_{polymer}}{\langle r_{polymer}\rangle_n} \quad (9)$$

where $\langle r_{polymer}\rangle_n$ is the number-averaged number of segments. Thus, N_{agg}^{eff} is the aggregation number of the micelle that would be noted *if* the occurrence of polydispersity were unknown.

In the following, the bulk volume fraction of component x, ϕ_x^b, will be referred to as the free volume fraction of component x, ϕ_x^{free}, and the excess amount as the amount being aggregated.

III. Polymer Model

Polymers. Pluronic polymers with a broad range of total mass and of EO/PO ratios are available commercially.

Table 1. Trademark[a] and Composition of Each of the Pluronic Block Copolymers Studied

trademark	M_{PPO}[b]	wt % EO[b]	composition
L64	1750	40	$(EO)_{13}(PO)_{30}(EO)_{13}$
P105	3250	50	$(EO)_{37}(PO)_{56}(EO)_{37}$
F127	4000	70	$(EO)_{106}(PO)_{69}(EO)_{106}$

[a] BASF Wyandotte Chemical Corp. [b] Data from manufacturer.

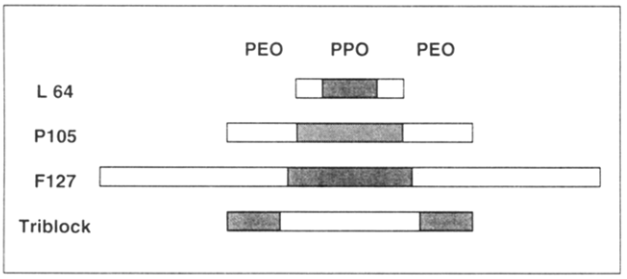

Figure 2. Schematic illustration of the molecular structure of the Pluronic P105 triblock copolymer and the impurities that were studied. The PEO blocks are represented by open areas, and the PPO blocks, by shaded areas. The length of each area is proportional to the number of monomers in the block.

(The EO/PO ratio will be referred to in the following as the composition of the polymer.) The synthesis procedure leads, however, to the formation of homopolymers and diblock copolymers (referred to as impurities) as well as to specific mass and composition distributions of the desired triblock copolymer. Aqueous solutions of Pluronic L64, P105, and F107 are used here to investigate the effects of polydispersity. In addition, a reversed Pluronic polymer, i.e., a triblock copolymer having a central PEO block and PPO blocks at the ends, of the same composition as Pluronic P105, is investigated. Table 1 gives the composition of the Pluronic triblock copolymers, and Figure 2 indicates schematically their molecular structure. Pluronic P105 and F127 were selected since model calculations for aqueous solutions of these polymers (neglecting the polydisperity in the model) have already been performed.[21,24,25] It was found in one of the previous investigations[21] that micelles of monodisperse Pluronic L64 polymers were not predicted by the model. In the present study it will be shown that polydisperse Pluronic L64 should indeed form micelles, as has also been observed experimentally.[3,6,8,16]

Interaction Parameters. In order to carry out the calculations, parameters describing the interaction among the species and the state equilibriums have to be specified. The internal state energy, U_{AB}, and the degeneration, g_{AB}, of all states of all species, as well as the Flory–Huggins interaction parameters between all pairs of species in the different states, $\chi_{BB'}$, are compiled in Table 2. All of them were determined earlier for simpler systems (for binary PEO/water,[33,34] binary PPO/water,[32] and ternary PEO/PPO/water solutions[35]) through fitting calculated phase diagrams to experimental ones. Therefore, in the present study there are no adjustable parameters. The set of parameters is the same as in the earlier investigations concerning the micellization of block copolymers containing EO and PO,[21] the phase behavior of Pluronic polymers in aqueous solution,[24] and the effect of polymer impurity on the micellization of Pluronic polymers.[25]

Polydispersity Model. Theoretical considerations indicate that the polymerization of a homopolymer from cyclic monomers with a fixed number of initiators gives a Poisson-distributed number (n) distribution.[36] The polydispersity expressed by the ratio of the mass to the number average of the molecular mass becomes then $M_m/M_n = 1 + \langle r\rangle_n/(1 + \langle r\rangle_n)^2$, where $\langle r\rangle_n$ is the n-averaged number of segments. For $\langle r\rangle_n \approx 50$, which is the case here, one obtains $M_m/M_n \approx 1.02$. However, the polydispersity in real situations is larger, at least 1.2, and the distribution is generally not well-known. Therefore, and for reasons of simplicity, all polydispersity calculations have been made by assuming a Schulz–Zimm distribution. In a recent work, Hecht used gel permeability chromatography to determine the polydispersity distribution of Pluronic F127, manufactured by BASF, Wyandotte Chemical Corp.[26] Hecht obtained a mass distribution resembling a Schulz–Zimm distribution but truncated at high masses. Using his measured distribution, a polydispersity ratio of 1.4 was obtained.

Table 2. Internal State Parameters (U_{AB} and g_{AB}) and Flory–Huggins Interaction Parameters ($\chi_{BB'}$) of the Theoretical Model (Energy in kJ mol^{-1})

state no.	species	state	U_{AB}	g_{AB}
1	water		0	1
2	EO	polar	0[a]	1[a]
3		nonpolar	5.086[a]	8[a]
4	PO	polar	0[b]	1[b]
5		nonpolar	11.5[b]	60[b]

	$kT\chi_{BB'}$			
state no.	2	3	4	5
1	0.6508[a]	5.568[a]	1.7[b]	8.5[b]
2		1.266[a]	1.8[c]	3.0[c]
3			0.5[c]	−2.0[c]
4				1.4[b]

[a] From the fit to the experimental data of the binary PEO/water phase diagram (see refs 33 and 34). [b] From the fit to the experimental data of the binary PPO/water phase diagram (see ref 32). [c] From the fit to the experimental data of the ternary PEO/PPO/water phase diagram (see ref 35).

The Schulz–Zimm distribution is normally expressed using two parameters related collectively to the average and the width of the distribution.[37] In the present case, it is more convenient to consider the distribution of a reduced number of segments, $x \equiv r/\langle r\rangle_n$, where r is the number of segments and $\langle r\rangle_n$ the n-averaged number of segments. The fraction of polymers having between r and $r + dr$ segments, $P_n(r)dr$, and the fraction of polymer segments that are in polymers having between r and $r + dr$ segments, $P_m(r)dr$, become $P_n(x)dx$ and $P_m(x)dx$, respectively, where

$$P_n(x) = k^k x^{k-1} \exp(-kx)/\Gamma(k) \tag{10a}$$

$$P_m(x) = k^{k+1} x^k \exp(-kx)/\Gamma(k+1) = xP_n(x) \tag{10b}$$

using the normalization expressions $\int_0^\infty P_n(x)\,dx = 1$ and $\int_0^\infty P_m(x)\,dx = 1$, and using $\langle x\rangle_n = 1$. The parameter k describing the width of the distribution is related to the standard deviation of $P_n(x)$, σ_n [$\sigma_n^2 \equiv \int_0^\infty (x-1)^2 P_n(x)\,dx$], by

$$k = (\sigma_n)^{-2} \tag{11}$$

Alternatively, k can be expressed in terms of the polydispersity ratio as

$$k = \left[\frac{M_m}{M_n} - 1\right]^{-1} \tag{12}$$

Thus, the smaller the k, the wider the distribution becomes. Most calculations were performed for $M_m/M_n = 1.2$, Figure 3a indicating the corresponding number and mass dis-

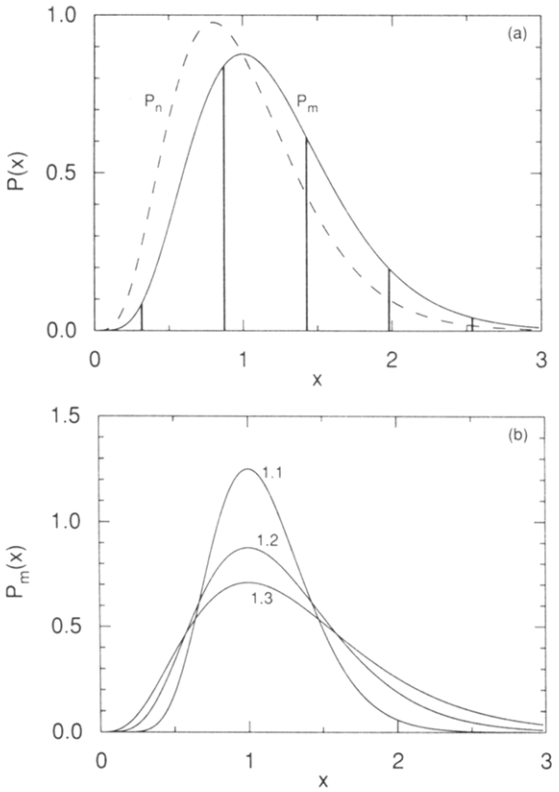

Figure 3. Schulz–Zimm distribution function used for describing polydispersity. $P(x)$ denotes the probability of $x \equiv r/\langle r\rangle_n$, where r is the number of segments in a polymer (or a block) and $\langle r\rangle_n$ the n-average number of segments of the polymer (or the block). (a) Number and mass distributions, $P_n(x)$ and $P_m(x)$, respectively, versus x for a polydispersity ratio of $M_m/M_n = 1.2$. (b) Mass distribution $P_m(x)$ versus x for $M_m/M_n = 1.1$, 1.2, and 1.3. A five-point discrete representation of $P_m(x)$ is shown in (a). The points were selected with constant spacing in x with $\langle x\rangle_n = 1$ and in a manner such that the same polydispersity as for the continuous representation was obtained.

tributions. Some calculations were also performed for $M_m/M_n = 1.1$ and 1.3, the corresponding mass distributions being given in Figure 3b.

A Pluronic polymer contains three blocks. If one assumes the blocks to be indepdent of each other, as regards the number of segments in each, there is in fact a three-dimensional polydispersity. In the model calculations, two different cases were examined. In the first, involving most of the calculations performed, the composition was held constant (fixed EO/PO ratio), only the total *mass* being allowed to vary. This situation is not fully realistic for real Pluronic polymer solutions. However, the computations are considerably simplified, and this less realistic model also enables one to investigate the effect of the sampling density on the Schulz–Zimm distribution (see below). In some cases, the number of segments in each block was varied independently, thus modeling *mass and composition* polydispersity.

The *mass* polydispersity was represented by treating polymer molecules with different numbers of segments as different components (cf. Figure 4a). The reduced number of segments of component j, x_j, and its related mass weight, w_j, were taken from the Schulz–Zimm distribution. Given the number of components, N_p, and the set $\{x_j, j = 1, 2, ..., N_p\}$, the weights were calculated according to $w_j = P_m(x_j)/\sum_{j'=1}^{N_p} P_m(x_{j'})$. For the polydispersity case in which $N_p \geq 2$, the members of the set $\{x_j\}$ were selected in increasing order such that $\langle x\rangle_n = 1$ and $x_j - x_{j-1} =$ constant, $j = 2, ..., N_p$, and that they yielded the desired polydispersity ratio M_m/M_n. The selection of $\{x_j\}$ required an

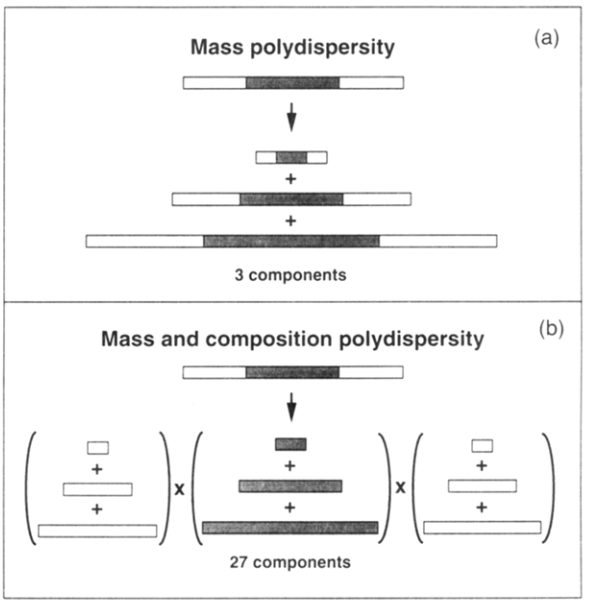

Figure 4. Illustration of the representation of polymer polydispersity in the model: (a) mass polydispersity and (b) mass and composition polydispersity. The polydisperse polymer is represented in (a) by several polymer components of equal composition and in (b) by a combination of blocks belonging to three different sets, each set representing a polydisperse PEO or PPO block. Pluronic P105 was employed. A polydispersity ratio of $M_m/M_n = 1.2$ and $N_p = 3$ were selected, and the lengths of the blocks are correctly scaled. The PEO blocks are represented by open areas and the PPO blocks by shaded areas.

iterative process. For the monodisperse case in which $N_p = 1$, it is obvious that $x = 1$, so that $r = \langle r\rangle_n$ was used. Table 3 gives the relative numbers of segments and the mass weights of the components employed in describing a polydisperse polymer for which $M_m/M_n = 1.2$ and $N_p = 2, ..., 5$. In Figure 3a, the $\{x_j\}$ obtained for $N_p = 5$ is shown graphically.

The final numbers of EO and PO segments of the polymer components are obtained by multiplying x_j by $\langle r_{EO}\rangle_n$ and $\langle r_{PO}\rangle_n$, identified as a and b, respectively, in the formula $(EO)_a(PO)_b(EO)_a$ in Table 1. Thus, the data from the manufacturer are treated as being n-averaged. (The manufacturer did not provide further detailed information when requested.) In the case of a mass polydispersity with $M_m/M_n = 1.2$ and represented by three polymer components, the components of Pluronic P105 would be $(EO)_{12}(PO)_{18}(EO)_{12}$, $(EO)_{40}(PO)_{61}(EO)_{40}$, and $(EO)_{69}(PO)_{104}(EO)_{69}$ having mass weights of 0.0783, 0.7041, and 0.2176, respectively. In the computations, the volume weights were taken to be equal to the mass weights.

For *mass and composition* polydispersity, the numbers of segments in each block were varied independently, the procedure as just described being applied to each block separately, the N_p taken being the same for each block (cf. Figure 4b). This yields $(N_p)^3$ number of components, but the inversion symmetry of the polymers reduces the number to $(N_p)^2(N_p + 1)/2$ distinguishable polymer components.

The results for the mass polydisperse polymers and for the mass and composition polydisperse polymers at the polydispersity ratio selected were roughly the same, differing considerably from the results for the monodisperse polymers. Hence, only a few results for mass and composition polydisperse polymers will be given, the presentation dealing primarily with the effect of mass polydispersity. The latter will in most cases be referred to simply as polydispersity.

Table 3. Relative Number of Segments, x_j, and Weights, w_j, of the N_p Polymer Components Describing a Polydisperse Polymer for $M_m/M_n = 1.2$[a]

	(x_j, w_j)				
N_p	$j = 1$	$j = 2$	$j = 3$	$j = 4$	$j = 5$
1	(1.000, 1.0000)				
2	(0.299, 0.0867)	(1.286, 0.9133)			
3	(0.328, 0.0783)	(1.093, 0.7041)	(1.859, 0.2176)		
4	(0.327, 0.0624)	(0.966, 0.5747)	(1.605, 0.2978)	(2.245, 0.0651)	
5	(0.317, 0.0482)	(0.872, 0.4714)	(1.427, 0.3452)	(1.981, 0.1114)	(2.536, 0.0239)

[a] $x_j \equiv r_j/\langle r\rangle_n$ where r_j is the number of segments of component j and w_j is its mass weight. $\langle r\rangle_n$ denotes the n-averaged number of segments and N_p the number of polymer components.

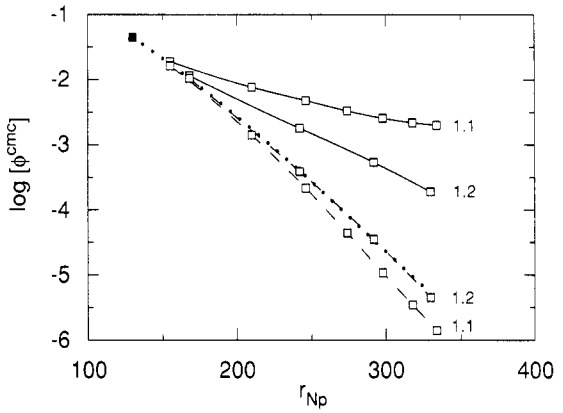

Figure 5. Polymer volume fractions (ϕ^{cmc}_{P105}) (solid curves with open squares) and the volume fractions of the longest polymer component ($\phi^{cmc}_{j=N_p}$) (dashed curves with open squares) at the cmc versus the number of segments of the longest polymer component ($r_{N_p} \equiv x_{N_p}\langle r_{P105}\rangle_n$) for an aqueous solution of Pluronic P105 with polydispersity ratios of $M_m/M_n = 1.1$ and 1.2 at $T = 320$ K. The symbols denote calculated points and the curves are fitted polynomials for increased readability. The largest number of components are $N_p = 8$ and 5, respectively. Also displayed is the polymer volume fraction at the cmc for aqueous solutions of monodisperse triblock copolymers of the same composition as Pluronic P105 versus the number of segments of the triblock copolymer (dotted curve). The filled square denotes the result for monodisperse Pluronic P105 ($r_{N_p} = 130$).

IV. Results and Discussion

Component Expansion. The polydisperse Pluronic polymer is represented by several polymer components which have different numbers of segments, their composition also differing in some cases. The convergence of some quantities with an increase in the number of polymer components, N_p, will be examined initially for solutions of Pluronic P105 of fixed composition at $T = 320$ K.

The model predicts that polymer micelles will be formed at a certain polymer concentration, the cmc, when the polymer concentration is increased to this point from zero.[21,31] Figure 5 shows, for polydispersity ratios $M_m/M_n = 1.1$ and 1.2, the total polymer volume fraction at the cmc, ϕ^{cmc}_{P105}, and the volume fraction of the polymer component with the *largest* number of segments, $\phi^{cmc}_{j=N_p}$ ($\equiv w_{N_p}\phi^{cmc}_{P105}$) as functions of the number of segments in the longest component, r_{N_p}. Also given in Figure 5, for the *total number* of segments as shown on the abscissa, is the cmc for a monodisperse polymer solution where the polymer has the same composition as Pluronic P105.

Consider first the case of $M_m/M_n = 1.2$. A comparison of monodisperse (the filled square at $N_p = 130$) and polydisperse Pluronic P105 (the solid curve labeled 1.2) shows the cmc to be reduced by several orders of magnitude as the polymer becomes polydisperse. Moreover, the cmc for the polydisperse case appears not to converge as N_p (and hence r_{N_p}) increases. Why is it so? The complete agreement between $\phi^{cmc}_{j=N_p}$ for the polydisperse model (the dashed curve labeled 1.2) and the cmc for the monodisperse model in which the polymer has a total number of segments equal to the number of segments of the longest component of the polydisperse model (dotted curve), indicates it to *only* be the aggregation properties of the longest component which determine the cmc for the polydisperse model. Clearly, ϕ^{cmc}_{P105} decreases with increasing N_p since x_{N_p}, and hence the number of segments of the longest polymer component, $r_{N_p} = x_{N_p}\langle r\rangle_n$, increases with N_p (cf. section III and Table 3).

The analysis can be continued one step further. Let the logarithmic behavior of $\phi^{cmc}_{j=N_p}$ observed (the dashed curve labeled 1.2) be expressed as

$$\ln \phi^{cmc}_{j=N_p} \approx -ar_{N_p} \tag{13}$$

which means that the logarithm of the volume fraction of the longest polymer component of the polydisperse model decreases linearly at cmc with the increasing number of segments in the longest component. Equation 10b shows that, for the limiting case of a large x and a small k, the weight of the components decays exponentially with x, i.e., $P_m(x) \approx \exp(-kx)$. Thus, for a solution of a polydisperse polymer we obtain to the leading order

$$\phi^{cmc}_{j=N_p} \approx P_m(x_{N_p})\phi^{cmc}_{P105} \approx \phi^{cmc}_{P105}\exp(-kx_{N_p}) \tag{14}$$

Combining eqs 13 and 14 gives

$$\ln \phi^{cmc}_{P105} \approx r_{N_p}(k/\langle r\rangle_n - a) \tag{15}$$

which indicates how the volume fraction of the polymer at the cmc depends on the number of segments in the longest component *and* on the degree of the polydispersity. Equation 15 shows that for $k/\langle r\rangle_n < a$, i.e., when the polydispersity is sufficient, the cmc decreases without limit as r_{N_p} increases. Thus, under the assumption that the logarithmic relationship presented in eq 13 is valid for larger N_p than investigated here, the exponential tail of the polydispersity distribution given in eq 10 and shown in Figure 3 should cause the cmc to approach zero. However, for a polydispersity ratio $M_m/M_n < 1 + 1/(a\langle r\rangle_n)$, the exponential tail would be sufficiently limited in the range to give a nonzero cmc even when N_p becomes infinite. Using the data for $M_m/M_n = 1.2$ given in Figure 5, one can estimate the crossover to occur at $M_m/M_n \approx 1.16$.

For a polydispersity ratio of $M_m/M_n \geq 1.3$, the logarithm of ϕ^{cmc}_{P105} also decreases linearly with N_p but with a larger slope, and $\phi^{cmc}_{j=N_p}$ versus N_p agrees completely with that for $M_m/M_n = 1.2$ (not shown). Hence, for $M_m/M_n = 1.3$ as well, the longest component determines the cmc, which is expected since the weights of the longer components increases as the polydispersity increases. In contrast, for a polydispersity ratio of $M_m/M_n = 1.1$, ϕ^{cmc}_{P105} appears to converge, albeit slowly, as N_p increases (see Figure 5), *and*

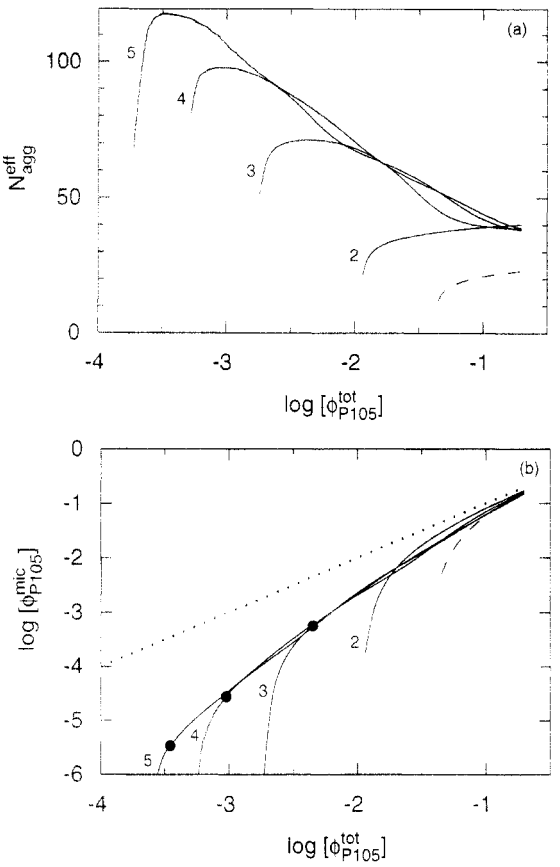

Figure 6. (a) Effective micellar aggregation number (N_{agg}^{eff}) and (b) micellar volume fraction (ϕ_{P105}^{mic}) versus the total polymer volume fraction (ϕ_{P105}^{tot}) at T = 320 K for an aqueous solution of polydisperse (solid curves) and monodisperse (dashed curve) Pluronic P105. The polydispersity ratio is M_m/M_n = 1.2, and the curves for the polydisperse system are labeled with the number of polymer components, N_p, representing the polydisperse polymer. In (a) the volume fraction at the left end of each curve corresponds to the cmc of the model system. In (b) the symbols on curves 3–5 denote the total polymer volume fraction where N_{agg}^{eff} displays its maximum. The vertical difference between ϕ_{P105}^{tot} (dotted curve) and ϕ_{P105}^{mic} represents the volume fraction of free polymers (ϕ_{P105}^{free}).

$\phi_{j=N_p}^{cmc}$ decreases faster (as compared with M_m/M_n = 1.2). Thus, for M_m/M_n = 1.1 both observations demonstrate the fact that it is not exclusively the longest component which determines the cmc, this supporting the analysis presented.

Figure 6a shows the effective aggregation number as a function of the total polymer volume fraction for a polydisperse Pluronic P105 for which N_p = 1, ..., 5 and M_m/M_n = 1.2. The left end of each curve corresponds to the cmc obtained from the model. The solution of the polydisperse polymer in which $N_p \geq 3$ has a prominent feature; viz. the effective aggregation number increases with the total polymer volume fraction when this is slightly above the cmc ($\phi_{P105}^{tot} \lesssim 1.5\phi_{P105}^{mic}$), whereas for higher volume fractions ($\phi_{P105}^{tot} \gtrsim 1.5\phi_{P105}^{mic}$) the effective aggregation number decreases, the maximum being reached at $\phi_{P105}^{tot} \approx 1.5\phi_{P105}^{mic}$. Moreover, there is a weak oscillation which is superimposed on the decrease, the number of oscillations increasing with N_p. Disregarding for the moment the initial rise and the weak oscillations at the higher volume fractions (which are both consequences of the discrete representation of the polydispersity distribution), the results for N_p = 3–5 appear to overlap each other reasonably well. Thus, one is tempted to conclude that at polymer volume fractions larger than that at which the effective aggregation number peaks, the effective aggregation number has essentially converged with respect to N_p.

Along with the total polymer volume fraction at the cmc, the micellar volume fraction at the cmc is likewise important for the discussion below. Figure 6b displays ϕ_{P105}^{mic} as a function of the total polymer volume fraction under the same conditions as before. At a high total polymer volume fraction most of the polymers are aggregated into micelles, whereas at lower volume fractions only a small fraction of the polymers are aggregated (note the double-logarithmic scale). Again, one can note that for $\phi_{P105}^{tot} > 1.5\phi_{P105}^{cmc}$ the curves for N_p = 3–5 superimpose upon each other. Thus, the segment $\phi_{P105}^{tot} \gtrsim 1.5\phi_{P105}^{cmc}$ of the curves ($N_p \geq 3$) should correspond to the converged micellar volume fraction. Regarding the cmc discussed in Figure 5, the data in Figure 6b suggest that (under the present conditions here) the micellar volume fraction at the cmc approaches zero as more and more of the exponential polydispersity tail is included ($N_p \to \infty$), as expected. For a solution of a monodisperse polymer, the present theory gives a *finite* micellar volume fraction at the cmc (cf. the left end of the dashed curve in Figure 6b and also refs 21 and 31).

One can already conclude, therefore, that polydispersity has a strong influence on micellization. Although a continuous polydispersity distribution is represented by a discrete one involving only a limited number of components, the results show that for M_m/M_n = 1.2 the quantities predicted for $\phi_{P105}^{tot} \gtrsim 1.5\phi_{P105}^{cmc}$ converge ($N_p \geq 3$). For a sufficiently high degree of polydispersity, ϕ_{P105}^{cmc} decreases logarithmically with increasing N_p. By increasing N_p, one is then able to probe arbitrary small polymer volume fractions, and by supplying a micellar volume fraction as a criterion of the cmc (further described below), one can determine the cmc. As shown in the following, one can also investigate how the size and structure of the micelles depends on, e.g., the temperature, the concentration, the degree of polydispersity, and the composition of the Pluronic triblock copolymers. For small polydispersity, the model gives a finite cmc (just as for a monodisperse polymer) which may be either smaller or larger than the detection limit supplied.

Finally, Wanka et al. have found experimentally that the logarithm of the cmc is proportional to the number of PO segments present when the number of EO groups is constant.[17] Figure 5 (dotted curve) shows that the logarithm of the cmc is proportional to the total number of segments at constant EO/PO composition. However, since the main effects arise from the number of PO segments, the two observations are very similar. Such a dependence of the cmc on the number of methylene groups is also typically found for a low molecular mass surfactant of the alkyl poly(ethylene oxide) type in aqueous solution.[38] Otherwise, in particular in the case of block copolymers in organic solvents, no such proportionally is found generally.[39]

Pluronic P105. Mass Polydispersity. (a) Micellar Structure. How the mass polydispersity affects micellar structure will now be examined in greater detail, using Pluronic P105 with a mass polydispersity ratio of M_m/M_n = 1.2 at 320 K.

It was concluded previously that it is the properties of the longest component(s) that determine the cmc. Thus, it can be anticipated that the volume fractions of the different components of the micelle (referred to as the micellar composition) differ from the overall composition. Figure 7a shows the fraction (by volume) of each polymer component as a function of the total polymer volume

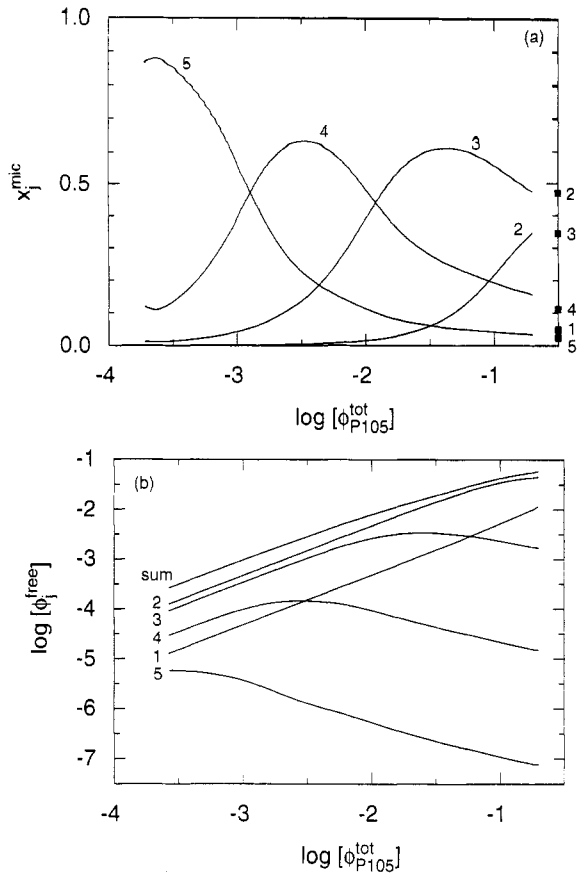

Figure 7. (a) Fraction of each polymer component in the micelle (x_j^{mic}) and (b) free volume fraction of each polymer component (ϕ_j^{free}) versus the total polymer volume fraction (ϕ_{P105}^{tot}) for an aqueous solution of polydisperse Pluronic P105 at 320 K. The polydispersity ratio is $M_m/M_n = 1.2$ and $N_p = 5$, the curves being labeled regarding the number of the component, j. In (a) $x_j^{mic} \equiv \Gamma_j/\sum_{j'} \Gamma_{j'}$, where Γ_j is the number of segments of polymer component j being aggregated. x_1^{mic} is too small to be visible, and the overall volume fractions are shown by the symbols on the right ordinate. In (b) the sum of the free volume fractions of the components, ϕ_{P105}^{free}, is also given (curve labeled "sum").

fraction. The figure clearly demonstrates the successive change in the major component as the volume fraction increases. Close to the cmc, almost 90% of the total polymer volume in the micelle consists of the longest polymer component. Even at the highest total polymer volume fraction, $\phi_{P105}^{tot} = 0.2$, the micellar composition has not yet reached the overall composition of the system. The smallest component, $j = 1$ (cf. also Figure 3), is too short to participate in the aggregation.

It is this change in the micellar composition and the finite number of components included in the model which cause the undulations in the effective aggregation numbers shown in Figure 6a and the weaker undulations in the micellar volume fraction in Figure 6b. The number of maxima increases with N_p, but the amplitude decreases as the difference in the length of adjacent components decreases. In a real system, the polydispersity distribution is for all practical purposes continuous, such oscillations being absent. However, for a well-characterized mixture consisting of only a few components of differing length, such oscillations should be possible to observe.

The free volume fractions of the polymer components are very strongly dependent on the total polymer volume fraction. Figure 7b shows that, whereas the free volume fractions of the two longest components are low and less dependent on the total polymer volume fraction, the two shortest ones display large increases. The intermicellar solution becomes progressively enriched in the shorter and deprived in the longest polymer components. Thus, at high concentrations the composition of the free polymers differs strongly from that at the cms at which the composition is close to the stoichiometric one. The volume fraction of free polymers (the top curve in Figure 7b) displays a steady increase as the total polymer volume fraction increases. This differs markedly from the case of a monodisperse polymer, in which the free polymer volume fraction is nearly constant above the cmc (see Figure 3 of ref 31 and Figure 6 of ref 21). A similar but less prominent difference between polydisperse and monodisperse polymers was obtained by Gao and Eisenberg using a thermodynamic model for mixed micelles that was applied to polydisperse polymers.[27]

On the basis of the theoretical approach employed, the radial volume fraction profiles of the EO and PO segments can be obtained using eq 2. Figure 8a shows these profiles for a polydisperse polymer at $\phi_{P105}^{tot} = 0.0005$ and 0.05, and for a monodisperse polymer at $\phi_{P105}^{tot} = 0.05$. In all three cases, the PO segments tend to be located at the core of the micelle and the EO segments in an outer layer. This is what one would expect as a result of solvency, since PPO is more hydrophobic than PEO. A comparison of the two models shows that the larger micelles formed in the polydisperse model are essentially due to the more extended central core involved, whereas the shapes of the density profiles of the outer regions are similar in the two cases. For the polydisperse model, growth of the micelle upon a reduction in the total polymer volume fraction is accompanied by a larger core region and by a more extended outer region. In the polydisperse model, the EO/PO separation becomes stronger, particularly at the lower total polymer volume fraction where the micelle is larger. For the monodisperse model, the EO/PO separation decreases when the total polymer volume fraction becomes less.

The volume fraction profile of each component in the polydisperse model is shown in Figure 8b. The figure shows in a more detailed way how the composition of the micelle changes with the total polymer volume fraction. At the lower concentration (solid curves), the longest component in the micelle clearly dominates, whereas at the higher concentration the micelles are largely formed of the more abundant middle components (cf. Figure 7a). In addition, a comparison of components 2–5 at $\phi_{P105}^{tot} = 0.05$ shows that the longer components are preferentially located at the core, whereas the shorter ones tend to be further out and their volume fraction profiles even display a maximum (the dashed curves labeled 2 and 3).

The model calculations also provide information on the spatial location of the EO–PO junctions of the different components (cf. eq 3). Figure 8c shows the volume fraction profiles of the EO–PO junctions of the monodisperse and polydisperse models at $\phi_{P105}^{tot} = 0.05$. As can be seen, the locations of the maxima of the profiles for the different components superimpose upon each other at $i = 10.1$. Also after the contribution of the free polymers has been subtracted, the junction profiles of the aggregated polymers are nearly proportional to each other.

Thus, from Figure 8b,c it can be concluded that chains of equal composition but of differing length are accommodated in the micelle in such a way that the EO–PO junctions of the different chains have similar radial distributions. This results in a maximum in the volume fraction profile of the shorter components through making it unlikely that the PO loops of the smaller chains will reach the center of the micellar core. Similarly, the outer

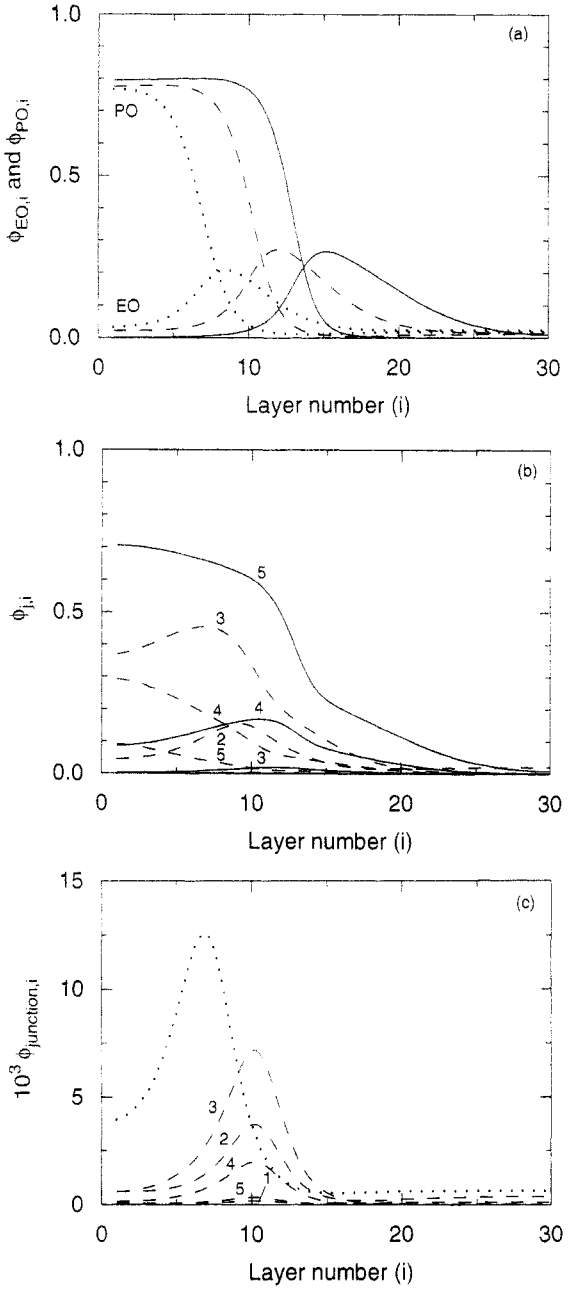

Figure 8. Volume fraction profiles (ϕ_i) versus the layer number (i) for an aqueous solution of polydisperse Pluronic P105 for a total polymer volume fraction $\phi^{tot}_{P105} = 0.05$ (dashed curve) and 0.0005 (solid curve) and of monodisperse Pluronic P105 for $\phi^{tot}_{P105} = 0.05$ (dotted curve) at $T = 320$ K. The polydispersity ratio is $M_m/M_n = 1.2$ and $N_p = 5$. (a) Segment volume fraction ($\phi_{EO,i}$ and $\phi_{PO,i}$). (b) Volume fraction of each polymer component ($\phi_{j,i}$). (c) Volume fraction of the EO–PO junctions of each polymer component ($\phi_{junction,i}$). In (b) not all components are visible since some $\phi_{j,i}$ are too small to be seen. In (b) the dotted curve is omitted, and in (c) the solid curves are omitted for clarity.

part of the EO layer, which consists predominantly of EO segments of the longer components, has a more extended tail (cf. Figure 8a). A comparison of the junction profiles of the monodisperse and polydisperse models shows that the volume fraction of junctions in the core of the micelle is much larger in the monodisperse model. Thus, polydispersity sharpens the separation of EO and PO, something which was also observed in Figure 8a.

Pluronic P105. Mass Polydispersity. (b) Temperature Dependence. The question of how the temperature affects various properties will now be dealt with, using again Pluronic P105 with a mass polydispersity ratio of $M_m/M_n = 1.2$.

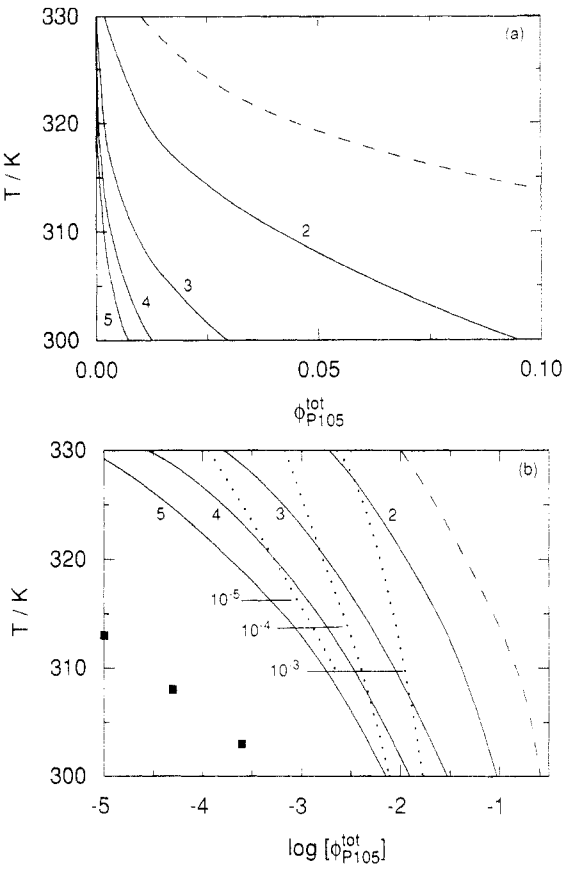

Figure 9. Critical micellar temperature (T) versus the total polymer concentration (ϕ^{tot}_{P105}) for an aqueous solution of polydisperse (solid curves) and monodisperse (dashed curve) Pluronic P105. The polydispersity ratio is $M_m/M_n = 1.2$. The curves for the polydisperse system are labeled in terms of the number of polymer components, N_p, representing the polydisperse polymer. (a) Linear concentration scale. (b) Logarithmic concentration-scale. In (b) (T, ϕ^{tot}_{P105}) points with constant micellar volume fractions (criterion of the cmc) are represented by dotted curves, the volume fractions being indicated. Experimental data from Alexandridis et al.[16a] are also included (filled squares).

A property of aqueous solutions of Pluronic polymers that is frequently investigated experimentally is the temperature dependence of the cmc or, alternatively, the concentration dependence of the critical micellar temperature (cmt).[16,17] In Figure 9a, the cmt is shown as a function of the total polymer volume fraction of Pluronic P105. For both the monodisperse and the polydisperse cases, as found experimentally as well, the cmt decreases as the polymer concentration increases. This effect is attributed to the reduction of the solubility of PPO and PEO as the temperature increases. For the polydisperse case, the cmt (cmc) decreases for all concentrations (temperatures) studied as N_p increases.

As discussed earlier, it appears that, for a polydispersity of sufficient degree, the cmc approaches zero for the continuous polydispersity distribution, making a finite representation of polydispersity here inadequate. However, as the number of polymer components increases, the micellar volume fraction at the cmc decreases (cf. Figure 6b). Hence, at some stage, the micellar volume fraction must fall below some limit, which would correspond to the experimental detection limit depending on the method employed. This has to be taken into account in comparing model predictions and experimental data.

Figure 9b shows the predicted cmt curves for micellar volume fractions of 10^{-5}, 10^{-4}, and 10^{-3}. Extensive determination of the cmt of Pluronic polymers in aqueous

solution has been performed by Alexandridis et al. through monitoring the change in the adsorption spectrum of a hydrophobic dye solubilized in the hydrophobic core of the micelle[16a] and by surface tension measurements,[16b] and they succeeded in obtaining consistent data from the two methods. Some of their data for Pluronic P105 are also included in Figure 9b. In the previous investigation,[21] the predicted cmc for a monodisperse model was found to be 20–30 K too high. On the basis of the experimental and the calculated data for the monodisperse system given in Figure 9b, the difference in the cmt for P105 Pluronic would be ≫30 K, or a difference of 3–4 orders of magnitude of the cmc, at a given temperature. A polydispersity ratio of $M_m/M_n = 1.2$ of the polymer improves the comparison with the experimental data considerably, but a difference of 1–2 orders of magnitude still remains when a detection level of 10^{-5} is employed as the criterion of the cmc. In order to make a more quantitative comparison, information on polydispersity and the presence of impurities has to be known as well as an assessment of the meaning of the cmc for the particular experimental methods employed.

Thus, the theory for a monodisperse polymer predicts a finite cmc at which the micelles start to appear in a finite concentration. On the other hand, in a sufficiently polydisperse system, both the predicted cmc and the micellar volume fraction at the cmc approach zero. In the latter case the meaning of the cmc (and cmt) has to be specified further. By using the criterion that the cmc denotes the concentration at which the micellar concentration attains some threshold value, one is again able to calculate a cmc of the model system. The same criterion would hold for the cmt. In fact, the polydisperse model, where a detection value needs to be specified, corresponds better to the experimental situation in which the cmc obtained generally depends on the technique used. Another approach, which also brings the model closer to the experimental case, is to use a truncated mass distribution, since after synthesis the high mass tail is normally removed.

For monodisperse polymers, it has been shown earlier[21] that, except for a rise just after the cmc, the aggregation number is nearly independent of the total polymer volume fraction (see also Figure 6a), but that the aggregation number increases strongly with temperature. For polydisperse polymers, as evident in Figure 10a, the effective aggregation number is also strongly temperature dependent but, in contrast (except for the initial rise), the effective aggregation number decreases with increasing total polymer concentration at all temperatures that were investigated. The aggregation numbers of the monodisperse and polydisperse models differ from each other at high volume fractions approximately by a factor of 2.

It is well established experimentally that Pluronic micelles grow increasingly as the temperature rises. Thus far, nevertheless, accurate experimental determinations of the aggregation number as a function of the polymer concentration are scarce. For a different system, however, poly(styrene-*block*-hydrogenated butadiene-*block*-styrene) in organic solvent, it has been found that the polymer micelles grow as the polymer concentration decreases and approaches the cmc. Tuzar et al. deduced from light-scattering measurements that the aggregation number of the micelles formed can be twice as large at cmc than at higher polymer concentrations.[40] The system they used was treated specially to remove homopolymer impurities, and the authors could not find any plausible explanation for this result. In view of the model results given in Figure 10a, a polydisperse polymer sample could be the explanation for the reduced micellar size found at increasing polymer concentrations.

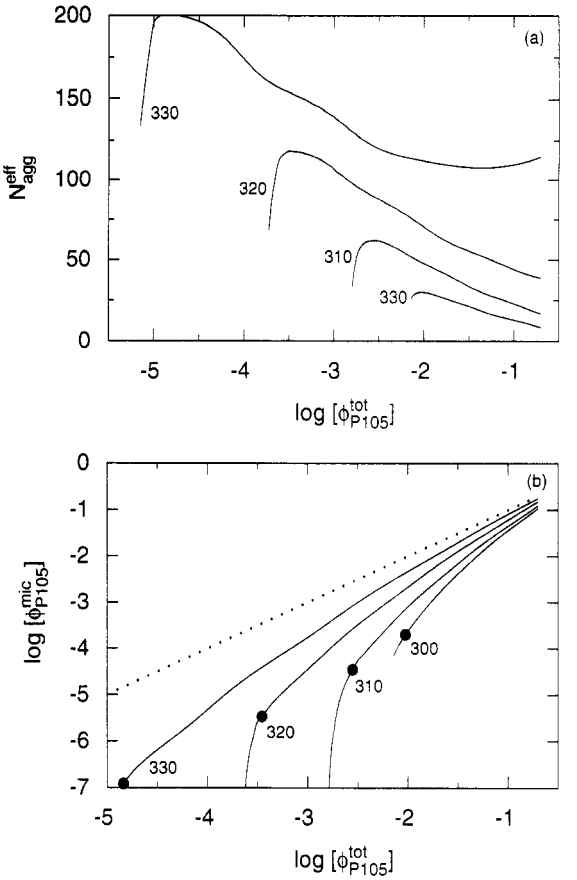

Figure 10. (a) Effective aggregation number (N^{eff}_{agg}) and (b) micellar volume fraction (ϕ^{mic}_{P105}) versus the total polymer volume fraction (ϕ^{tot}_{P105}) for an aqueous solution of polydisperse Pluronic P105 at T = 300, 310, 320, and 330 K. The polydispersity ratio is $M_m/M_n = 1.2$ and $N_p = 5$. In (b) the symbols denote the total polymer volume fraction where N^{eff}_{agg} displays its maximum.

Figure 10b shows the micellar volume fraction, and hence indirectly the volume fraction of free polymers, likewise as a function of the total polymer volume, at different temperatures. For polymer volume fractions above the one at which the effective aggregation number has its maximum, the power dependence is $\phi^{mic}_{P105} \approx$ const $[\phi^{tot}_{P105}]^{\alpha}$, the exponent α ranging from 1.5 at 330 K to 2.0 at 330 K. For $N_p > 5$, this approximate relationship can be expected to continue on to lower volume fractions than those shown. The figure indicates, e.g., that for $\phi^{tot}_{P105} = 0.01$ and at 300 K, only about 2% of the polymers are aggregated, whereas at 330 K about 50% of them are aggregated. Again, this is a demonstration of the decreasing solubility of the Pluronic polymers at increasing temperature.

Pluronic P105. Mass Polydispersity. (c) Polydispersity Dependence. As already indicated, the cmc is reduced as the polydispersity increases. Figure 11 displays the relationship between the total polymer volume fraction at the cmc and the polydispersity ratio for different detection limits being the criterion of the cmc. Thus, a quantitative prediction can be made of how the cmc changes with the degree of polydispersity found at different detection levels. For example, a polydispersity of $M_n/M_n = 1.1$ reduces the cmc by a factor of 20 at the lowest detection limit considered and by a factor of 4 at the highest, as compared with a monodisperse polymer. An increase in polydispersity to 1.2 causes a reduction in the cmc by factors of 160 and 7, respectively, at the lowest and highest detection limits considered.

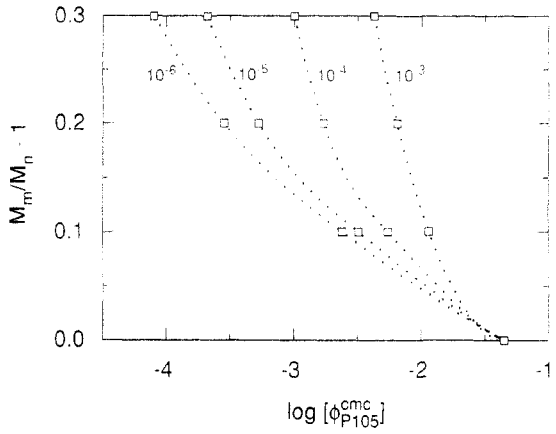

Figure 11. Polydispersity ratio (M_m/M_n) versus the total polymer volume fraction (ϕ^{mic}_{P105}) at different micellar volume fractions (criterion of the cmc) for Pluronic P105 at T = 320 K. The calculations were performed for N_p = 5. The symbols denote the calculated points, whereas the curves are fitted polynomials for increased readability.

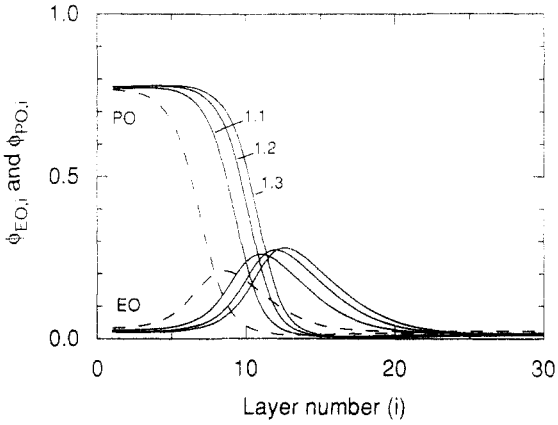

Figure 12. Segment volume fraction profiles ($\phi_{EO,i}$ and $\phi_{PO,i}$) versus the layer number (i) for an aqueous solution of polydisperse (solid curves) and monodisperse (dashed curve) Pluronic P105 for a total polymer volume fraction ϕ^{tot}_{P105} = 0.05 at T = 320 K. The effective aggregation numbers N^{eff}_{agg} are 15.60, 38.24, 51.23, and 60.35, for the polydispersity ratios M_m/M_n = 1, 1.1, 1.2, and 1.3, respectively. The calculations were performed for N_p = 5.

The model calculations thus predict that the polydispersity has a strong influence on the cmc and that the effect increases as the micellar volume fraction used to define the cmc becomes lower. These results suggest that knowledge of the polydispersity is of paramount importance in comparing results pertaining to different batches of a polymer or results pertaining to different members of the Pluronic family. The effect of the polydispersity has not thus far been examined thoroughly *per se*.

At a given temperature, the effective aggregation number increases with the polydispersity ratio. For an aqueous solution of Pluronic polymer with ϕ^{tot}_{P105} = 0.05 at T = 320 K, the effective aggregation number increases from 15.6 to 38.2, 51.2, and 60.4 as the monodisperse polymer becomes polydisperse with ratios of M_m/M_n = 1.1, 1.2, and 1.3, respectively. The corresponding segment volume profiles are shown in Figure 12. Thus, with increasing polydispersity, there is a continuous increase in the aggregation number as well as in the micellar size. For M_m/M_n = 1.2, polydispersity causes a 3-fold increase in the effective aggregation number, with a concomitant increase in micellar size.

The effect on micellization of the presence of polymer impurities has been studied with the same model.[25] In the case of an aqueous solution of monodisperse Pluronic P105 in which 5% of the polymer mass was a PEO–PPO diblock impurity, the reduction in the cmc was only moderate. The reduction depended largely on the temperature, but was ca. 30% at 320 K. Similarly, the increase in the effective aggregation number was small. Thus, it seems that polydispersity has a larger influence on the aggregation of Pluronic P105 than diblock impurities do. The presence of a small amount of PPO homopolymer impurity also leads to only a moderate reduction in the cmc, yet close to the solubility limit of the PPO impurity the effective aggregation number can increase by a factor of 2,[25] a change comparable with the effect of polydispersity.

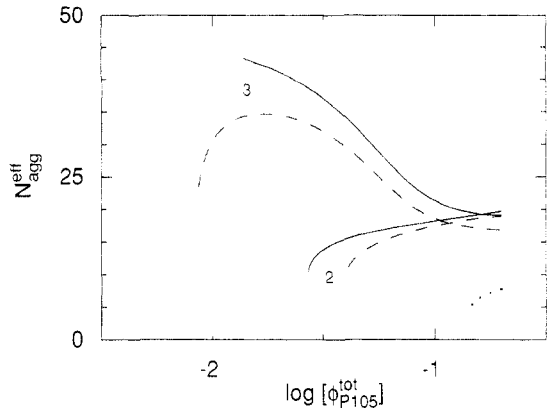

Figure 13. Effective aggregation number (N^{eff}_{agg}) versus the total polymer volume fraction (ϕ^{tot}_{P105}) at T = 310 K for an aqueous solution of mass and composition polydisperse (solid curves), mass polydisperse (dashed curves), and monodisperse (dotted curve) Pluronic P105. The polydispersity ratio is M_m/M_n = 1.2. The curves for the polydisperse systems are labeled in terms of the number of components, N_p, representing one polydisperse block and the polydisperse polymer, respectively.

Pluronic P105. Mass and Composition Polydispersity. The effect of mass and composition polydispersity, as described in section III, was investigated by modeling aqueous solutions of Pluronic P105. Figure 13 shows the effective aggregation number as a function of the total polymer volume fraction for a monodisperse polymer, for a mass polydisperse polymer at M_m/M_n = 1.2, and for a mass and composition polydisperse polymer having a polydispersity ratio of M_m/M_n = 1.2 for each block. For the polydisperse cases, N_p = 2 and 3 were examined, corresponding to 6 and 18 distinguishable polymer components, respectively, for the case of the mass and composition polydispersity. As indicated previously, the left end of each curve corresponds to the predicted cmc of the model. [In the case of mass and composition polydispersity at N_p = 3, the failure to obtain a converged solution at a ϕ^{tot}_{P105} smaller than indicated in Figure 13 occurred probably prior to the cmc being reached. Despite extensive investigations, the origin of this absence of convergency could not be determined conclusively.] Figure 13 shows that the additional composition polydispersity increases the effective aggregation number somewhat and that it reduces the cmc (at least for N_p = 2). However, the main effect, as compared with the monodisperse model, is already shown to be present by the use of a mass polydisperse model.

The segment density profiles for ϕ^{tot}_{P105} = 0.05 at N_p = 3 were compared. Figure 14 indicates that the larger aggregation number obtained for the mass and composition polydisperse model causes the EO and PO profiles to extend further outward. However, in the core, the volume fraction of PO is reduced and of EO increased by ca. 0.03, giving the same total polymer volume fraction. The EO–

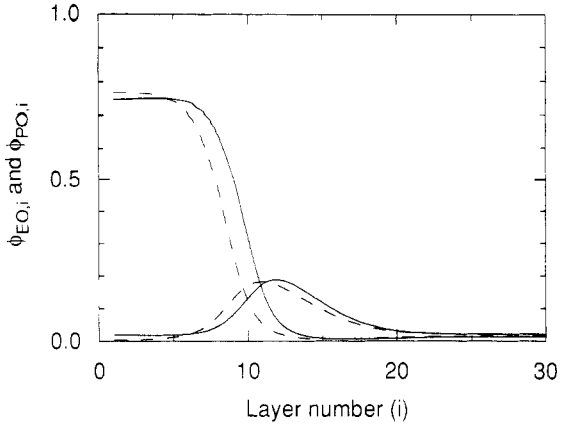

Figure 14. Segment volume fraction profiles ($\phi_{EO,i}$ and $\phi_{PO,i}$) versus the layer number (i) for an aqueous solution of mass and composition polydisperse (solid curves) and mass polydisperse (dashed curve) Pluronic P105 for a total polymer volume fraction $\phi^{tot}_{P105} = 0.05$ at $T = 310$ K. The effective aggregation numbers N^{eff}_{agg} are 30.60 and 25.56, respectively. The polydispersity ratio is $M_w/M_n = 1.2$ and $N_p = 3$.

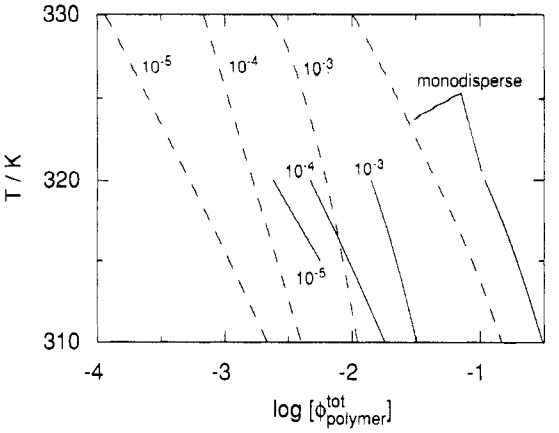

Figure 15. Critical micellar temperature (T) versus the total polymer concentration (ϕ^{tot}_{P105}) at different micellar volume fractions (criterion of the cmc) for an aqueous solution of a PPO–PEO–PPO triblock copolymer (solid curves). The polydispersity ratio is $M_w/M_n = 1.2$ and $N_p = 5$. The cmt for the monodisperse polymer is also shown (solid curve). The triblock copolymer has the same composition as Pluronic P105; see Figure 2. The corresponding data for an aqueous solution of Pluronic P105 are also shown (dashed curves).

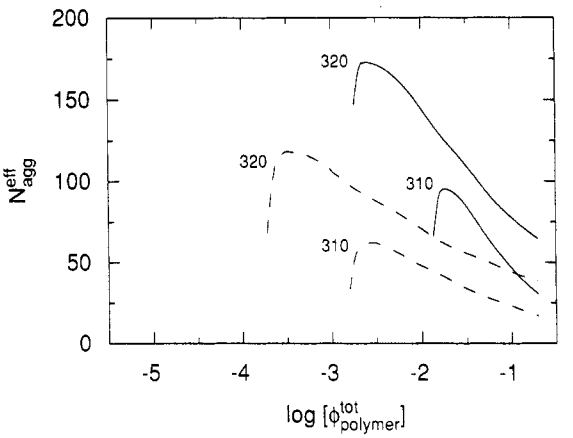

Figure 16. Effective aggregation number (N^{eff}_{agg}) versus the total polymer volume fraction (ϕ^{tot}_{P105}) for an aqueous solution of a PPO–PEO–PPO triblock copolymer (solid curves) at $T = 310$ and 320 K. The polydispersity ratio is $M_w/M_n = 1.2$ and $N_p = 5$. The triblock copolymer has the same composition as Pluronic P105; see Figure 2. The corresponding data for an aqueous solution of Pluronic P105 are also shown (dashed curves).

PO junction volume fraction profiles of the six most abundant components in the micelle had their peaks within 0.5 layers (data not shown). The junction profiles of the two components with one short PEO block, $(EO)_{12}(PO)_{61}(EO)_{40}$ and $(EO)_{12}(PO)_{104}(EO)_{40}$, respectively, also had clear maxima located in the center of the micelle. Thus, for entropic reasons these short PEO blocks are located partly in the PO core, resulting in the less distinct EO–PO separation mentioned above.

Accordingly, complete three-dimensional polydispersity appears to slightly extend the effects observed for mass polydisperse polymers. However, this conclusion is somewhat uncertain, since only limited comparisons were performed and numeric convergency difficulties may have arisen.

Reversed Pluronic P105. It was found earlier that a monodisperse triblock copolymer of the same composition as P105, but with a central PEO block and two equal PPO end blocks (see Figure 2), likewise forms micelles in aqueous solution.[21] The cmc was about twice as high as that and the temperature range of stable micelles smaller than that for Pluronic P105. In addition, at the single temperature that was investigated, the aggregation number was found to be larger.

The influence of polydispersity on the micellization of the PPO–PEO–PPO triblock copolymer was investigated in the same manner as for Pluronic P105. Figure 15 shows the critical micellar temperature as a function of the total polymer volume fraction for different micellar volume fractions, using aqueous solutions of the PPO–PEO–PPO triblock copolymer and of Pluronic P105 at a mass polydispersity ratio of $M_w/M_n = 1.2$. The micelles formed by the monodisperse triblock copolymer were not stable above $T \approx 320$ K, and polydispersity did not alter this instability temperature. Polydispersity caused a reduction in the cmc at a fixed temperature in a manner similar to that for Pluronic P105, although the effect was not as prominent. This led to a ratio of the cmc for the triblock copolymer and Pluronic P105 increasing from 2 (monodisperse polymer) to 5 for the polydisperse polymers at a detection level of $\phi^{mic}_{P105} = 10^{-5}$.

The effective aggregation numbers for these same systems are displayed in Figure 16. For the PPO–PEO–PPO triblock copolymer too, polydispersity leads to the effective aggregation number having a concentration dependence different from that in a monodisperse system (cf. Figure 6a). Under all the conditions shown, it is the PPO–PEO–PPO triblock copolymer which has the larger effective aggregation number and for which the effective aggregation number increases more rapidly with a decrease in the total polymer volume fraction.

Pluronic L64. For a given temperature, both the experiments and the theory predict that the cmc will increase with decreasing mass and with an increase in the PO content of the Pluronic polymers.[16,21] Pluronic L64 (structure given in Figure 2) is the shortest member of the Pluronic family reported to form micelles in aqueous solution. The previous investigation of the micellization of monodisperse Pluronic polymers failed to predict the existence of micelles of Pluronic L64.[21] It was concluded that the discrepancy between experiment and theory might possibly be attributed to polydispersity in the experimental system.

Model calculations using $N_p = 5$ and a polydispersity ratio of $M_w/M_n = 1.3$ yielded locally stable micelles, whereas a ratio of 1.2 was not sufficient for micelles to be obtained. The temperature interval for stable micelles was narrow, 314–319 K, and the total polymer volume

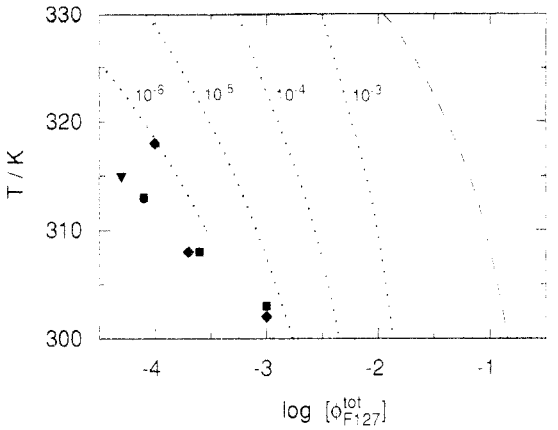

Figure 17. Critical micellar temperature (T) versus the total polymer concentration (ϕ^{tot}_{P105}) at different micellar volume fractions (criterion of the cmc) for an aqueous solution of Pluronic F127 (dotted curves). The polydispersity ratio is $M_m/M_n = 1.2$ and $N_p = 7$. The cmt for a monodisperse polymer is also shown (dashed curve). Experimental data from Alexandridis et al.[16a] (filled squares), Wanka et al.[17] (filled nabla), and Linse and Malmsten[20] (filled diamonds) are also included.

fraction was always in the range 0.02–0.2. The qualitative dependence of the effective aggregation number on the total polymer volume fraction differed too; the aggregation number increased continuously with the total polymer volume fraction until the micelles became unstable due to a catastrophic increase in size.

In the model calculations, the presence of polydispersity thus extends the mass and composition range of the Pluronic polymers for which micelles may occur. This brings the experimental and theoretical observations closer to each other.

Pluronic F127. The longest and most hydrophilic Pluronic polymer considered is F127. It contains 70% EO and has a molecular mass of ca. 13 000 g mol^{-1}. It forms micelles in aqueous solutions readily and has been the subject of several investigations.[1,2,16,17,20,21] For Pluronic F127 in aqueous solution, a monodisperse model has also been found to give too large a cmc, as compared with experimental data (Figure 7 of ref 21).

Figure 17 shows the predicted cmts for an aqueous solution of Pluronic F127 with a polydispersity ratio $M_m/M_n = 1.2$ at different micellar volume fractions, being the criterion of the cmc. The polydispersity gives a somewhat larger reduction in the cmc than it does for Pluronic P105. Additional experimental data, from Alexandridis et al. using the solubilization of due species,[16a] from Wanka et al. using surface tension measurements,[17] and from Linse and Malmsten using surfaces tension measurements and ellipsometry,[20] are also in included in Figure 17. Reasonable agreement among the experimental data is evident.

It is also evident that the agreement between the experimental and theoretical data is dramatically improved when polydispersity is included in the model. For the values $M_m/M_n = 1.2$ and $\phi^{mic}_{F127} = 10^{-6}$ that were selected as the criterion of the cmc, semiquantitative agreement was obtained. This does not necessarily imply that the individual values for M_m/M_n and ϕ^{mic}_{F127} were those that best represent the experimental situation. Other combinations would be likely to give similar agreement. A polydispersity ratio of 1.4 was deduced from the mass distribution obtained from a gel permeability chromatography study[26] of Pluronic F127 (see section III).

V. Summary

The micellization of polydisperse triblock copolymers consisting of EO and PO segments was investigated on the basis of a lattice theory for polymer solutions in heterogeneous systems. The polydisperse polymer sample was represented by several polymer components, each of which was of different length (and composition). The polydispersity was assumed to follow the Schulz–Zimm distribution. The inverse temperature behavior occurring in the phase diagram of aqueous PEO and PPO solutions was taken into account by allowing the polymer segments to adopt different states depending upon the temperature and concentration of the solutions. The effective segment–segment interaction became both concentration and temperature dependent, the latter being essential for describing the temperature dependence of the cmc. All the interaction parameters employed were ones derived independently in previous investigations of the phase diagrams of simpler systems. Thus, no adjustable parameters were involved in the study.

The single most important result appears to be that the polydispersity strongly facilitates micellization. The other major conclusions are as follows.

(1) The results obtained for mass polydisperse polymers and for mass and composition polydisperse polymers seemed to be quite similar. Although the following conclusions are based on results for mass polydisperse polymers only, similar conclusions could be expected for mass and composition polydisperse polymers.

(2) It appears that a polydisperse polymer and its self-aggregation can be adequately described using only a limited number of components. The constraint of sequentially equal differences in the mass of the components yielded a well-behaved variation of the different properties of the polymer as the number of components was increased.

(3) The theory predicts a finite micellar volume fraction for a monodisperse polymer. This seems to also be the case for a moderately polydisperse polymer, whereas for a polymer with greater polydispersity, the cmc, and hence the micellar volume fraction at the cmc, approaches zero as the number of polymer components describing the Schulz–Zimm distribution is increased.

(4) The relative volume fraction of different polymer components in the micelle depends strongly on the polymer concentration. Close to the cmc, the micelles are predominantly formed by the longest/most hydrophobic polymer component.

(5) The effective aggregation number is reduced with increasing polymer concentration, a behavior which is the opposite of that for a monodisperse polymer.

(6) The cmc decreases by several orders of magnitude and the effective aggregation number increases by about a factor of 2 for a polydispersity ratio of 1.2. These effects increase as the polydispersity ratio becomes still greater. The strong temperature dependencies found for the monodisperse polymers are likewise found for polydisperse polymers.

A comparison of the theoretical results with experimental data shows that agreement improves considerably when polydispersity is included in the model. Particularly notable is the much closer agreement this gives of the cmc (and of the cmt). A polydisperse model of Pluronic L64 was found to form micelles, whereas a monodisperse model did not. The reduction in the aggregation number at increasing polymer concentration obtained on the basis of the polydisperse model appears not to have been experimentally documented for Pluronic polymer systems. Polydispersity seems to have a larger effect on the cmc and on the size of the micelles formed than polymer impurities do. In order to carry out further quantitative comparisons, additional information on the polydispersity

of the polymers would be required and an assessment of the meaning of the cmcs for those particular experimental methods employed has to be made.

Despite the large improvement between the experimental data and the theoretical predictions achieved here, other simplications of the model system may still be important. Likely candidates are the mean-field approximation which suppresses the concentration fluctuations in each layer and the inherent assumptions in the lattice approach. Moreover, the thermodynamic model of the micellization neglects size, shape, and composition fluctuations of the micelles. These fluctuations tend to reduce the predicted cmc.

Acknowledgment. W. Ulbricht and E. Hecht are gratefully acknowledged for their helpful correspondence concerning the polydispersity of Pluronic polymers, and A. Hatton and H. Hoffmann for their providing preprints of their investigations prior to publication. This work was supported by the Swedish Research Council for Engineering Science (TFR).

References and Notes

(1) Rassing, J.; Attwood, D. *Int. J. Pharm.* **1983**, *13*, 47.
(2) Attwood, D.; Collett, J. H.; Tait, C. J. *Int. J. Pharm.* **1985**, *26*, 25.
(3) Zhou, A.; Chu, B. *Macromolecules* **1988**, *21*, 2548.
(4) Zhou, Z.; Chu, B. *J. Colloid Interface Sci.* **1988**, *126*, 171.
(5) Wanka, G.; Hoffmann, H.; Ulbricht, W. *Colloid Polym. Sci.* **1990**, *268*, 101.
(6) Reddy, N. K.; Fordham, P. J.; Attwood, D.; Booth, C. *J. Chem. Soc., Faraday Trans.* **1990**, *86*, 1569.
(7) Brown, W.; Schillén, K.; Almgren, M.; Hvidt, S.; Bahadur, P. *J. Phys. Chem.* **1991**, *95*, 1850.
(8) Almgren, M.; Bahadur, P.; Jansson, M.; Li, P.; Brown, W.; Bahadur, A. *J. Colloid Interface Sci.* **1992**, *151*, 157.
(9) Malmsten, M.; Lindman, B. *Macromolecules* **1992**, *25*, 5440.
(10) Brown, W.; Schillén, K.; Hvidt, S. *J. Phys. Chem.* **1992**, *96*, 6038.
(11) Hurter, P. N.; Hatton, T. A. *Langmuir* **1992**, *8*, 1291.
(12) Mortensen, K. *Europhys. Lett.* **1992**, *19*, 599.
(13) Mortensen, K.; Brown, W. *Macromolecules* **1993**, *26*, 4128.
(14) Mortensen, K.; Pedersen, J. S. *Macromolecules* **1993**, *26*, 805.
(15) Fleischer, G. *J. Phys. Chem.* **1993**, *97*, 517.
(16) (a) Alexandridis, P.; Holzwarth, J. F.; Hatton, T. A. *Macromolecules* **1994**, *27*, 2414. (b) Alexandridis, P.; Athanassiou, V.; Fukuda, S.; Hatton, T. A. *Langmuir* **1994**, *10*, 2604.
(17) Wanka, G.; Hoffmann, H.; Ulbricht, W. *Macromolecules* **1994**, *27*, 4145.
(18) Zhang, K.-W.; Khan, A. *Macromolecules*, submitted for publication.
(19) Nagarajan, R.; Ganesh, K. *J. Chem. Phys.* **1989**, *90*, 5843.
(20) Linse, P.; Malmsten, M. *Macromolecules* **1992**, *25*, 5434.
(21) Linse, P. *Macromolecules* **1993**, *26*, 4437.
(22) Hurter, P. N.; Scheutjens, J. M. H. M.; Hatton, T. A. *Macromolecules* **1993**, *26*, 5030.
(23) Hurter, P. N.; Scheutjens, J. M. H. M.; Hatton, T. A. *Macromolecules* **1993**, *26*, 5592.
(24) Linse, P. *J. Phys. Chem.* **1993**, *97*, 13896.
(25) Linse, P. *Macromolecules* **1994**, *27*, 2685.
(26) Hecht, E. Diplomarbeit, Bayreuth, 1993.
(27) Gao, Z.; Eisenberg, A. *Macromolecules* **1993**, *26*, 7353.
(28) Fleer, G. J.; Cohen Stuart, M. A.; Scheutjens, J. M. H. M.; Cosgrove, T.; Vincent, B. *Polymer at Interfaces*; Champan & Hall: London, 1993.
(29) Roefs, S. P. F. M.; Scheutjens, J. M. H. M.; Leermakers, F. A. M. *Macromolecules* **1994**, *27*, 4810.
(30) Scheutjens, J. M. H. M.; Fleer, G. J. *J. Phys. Chem.* **1979**, *83*, 1619; **1980**, *84*, 178.
(31) van Lent, B.; Scheutjens, J. M. H. M. *Macromolecules* **1989**, *22*, 1931.
(32) Linse, P.; Björling, M. *Macromolecules* **1991**, *24*, 6700.
(33) Karlström, G. *J. Phys. Chem.* **1985**, *89*, 4962.
(34) Björling, M.; Linse, P.; Karlström, G. *J. Phys. Chem.* **1990**, *94*, 471.
(35) Malmsten, M.; Linse, P.; Zhang, K.-W. *Macromolecules* **1993**, *26*, 2905.
(36) Flory, P. J. *Principles of Polymer Chemistry*; Cornell University Press: Ithaca, NY, 1953.
(37) *Polymer Handbook*; Brandrup, J., Immergut, E. H., Eds.; Wiley: New York, 1989.
(38) Lindman, B.; Wennerström, H. *Top. Curr. Chem.* **1980**, *87*, 1.
(39) Astafieva, I.; Zhong, X. F.; Eisenberg, A. *Macromolecules* **1993**, *26*, 7339.
(40) Tuzer, Z.; Stepanek, P.; Cestmír, K.; Kratochvíl, P. *J. Colloid Interface Sci.* **1985**, *105*, 372.